Sensors & Actuators: B. Chemical 399 (2024) 134751

Contents lists available at ScienceDirect

Sensors and Actuators: B. Chemical

journal homepage: www.elsevier.com/locate/snb

Extrinsic oxygen defects in SnO/SnO_2 heterostructure for efficient NO_2 gas detection

Jihee Kim [a,1], Masoud Nazarian-Samani [a,1], Jihyun Lee [a], Sang-kil Lee [a], Ji Hee Pi [a], Kyu Hyong Lee [a], Yu Jin Kim [a,b,*], Sanghyeon Lee [b,**], Wooyoung Lee [a,**]

[a] Department of Materials Science and Engineering, Yonsei University, 50 Yonsei-ro, Seodaemun-gu, Seoul 03722, South Korea
[b] KIURI Institute, Yonsei University, 50 Yonsei-ro, Seodaemun-gu, Seoul 03722, South Korea

ARTICLE INFO

Keywords:
Tin-oxide gas sensor
NO_2 gas sensor
SnO/SnO_2 heterostructure
Oxygen vacancy
NO_2 selectivity

ABSTRACT

High selectivity and fast response in the detection of NO_2 are key factors in protecting human health in life-threatening environments. The p-n SnO/SnO_2 heterostructure is a promising material as a metal oxide for effective chemical reactions with a target gas. It has a synergistic effect on the intrinsic semiconducting properties and the formation of an interfacial electric field in the heterojunction. The extrinsic oxygen vacancies in the SnO/SnO_2 structure enhance the chemical reaction in the sensing property. In this study, we developed a defect-SnO/SnO_2 heterostructure-based NO_2 gas sensor. It shows excellent sensing performances with a high response of 100.86, fast response time of 5.83 s, and superior selectivity (approximately 23 times higher than those of other target gases) in the detection of 50 ppm NO_2 at 150 °C. Raman and electron paramagnetic resonance (EPR) results supported the presence of oxygen vacancies in the defect-rich SnO/SnO_2 crystal and X-ray photoelectron spectroscopy (XPS) and time-of flight secondary ion mass spectrometry (ToF-SIMS) analyses described the role of SnO/SnO_2 heterostructure with oxygen defects as an effective electron donor for the adsorbed oxygen molecules and NO_2 target gas. We believe that the direct formation of oxygen vacancies in the SnO/SnO_2 heterostructures is a significant reference for the development of high-performance NO_2 gas sensors.

1. Introduction

Rapid industrialization and population growth have caused significant air pollution with toxic gases, resulting in serious environmental and health problems. Among the toxic gases, nitrogen dioxide (NO_2) is one of the most hazardous and is mainly produced by vehicles, factories, and power plants via combustion at high temperatures [1–3]. The Health and Safety Rule Alarm has caused that the human body should avoid staying for over 8 h in an NO_2 environment with 3 ppm [4]. The fast recognition and selective detection of NO_2 gas, in particularly at the low concentrations, is the only way to protect human health in life-threatening environments. Therefore, the development of NO_2 gas sensors with a fast response and high selectivity is essential.

As chemiresistive NO_2 sensors, tin (II or IV) oxide-based devices have been actively developed by the sensor research community as its intrinsic semiconducting property. Tin (II) oxide (SnO) is a p-type semiconductor with a band gap range of 2.5–3.4 eV [5] including intrinsic Sn vacancies [6], whereas tin (IV) oxide (SnO_2) is a typical n-type semiconductor with a wide band gap of 3.6 eV [7]. When combined with a heterostructure, that is, an SnO/SnO_2 p-n junction, electrons transfer from SnO_2 (high Fermi level) to SnO (low Fermi level) until equilibrium is reached [8]. This phenomenon led to the formation of an interfacial electric field in the SnO/SnO_2 heterojunction. This allows for a decrease in the required energy for electron transitions, providing two benefits. First, it becomes easy to reduce the adsorbed oxygen molecules of O_2 to O_2^-, which facilitates an effective chemical interaction with the NO_2 target gas [9,10]. Secondly, NO_2 gas can be directly adsorbed onto the surface of the heterostructure, making it easy to reduce NO_2 to NO_2- species [9,11,12]. Thus, for gas-sensing properties, the response sensing level and response/recovery transient times can be boosted.

SnO/SnO_2 p-n heterojunctions can be easily synthesized via a simple

* Corresponding author at: Department of Materials Science and Engineering, Yonsei University, 50 Yonsei-ro, Seodaemun-gu, Seoul 03722, South Korea.
** Corresponding authors.
E-mail addresses: yujin.kim@yonsei.ac.kr (Y.J. Kim), sha1140@yonsei.ac.kr (S. Lee), wooyoung@yonsei.ac.kr (W. Lee).
[1] Jihee Kim and Masoud Nazarian-Samani equally contributed.

https://doi.org/10.1016/j.snb.2023.134751
Received 4 August 2023; Received in revised form 26 September 2023; Accepted 8 October 2023
Available online 12 October 2023

oxidation process from SnO without additional procedures [8,13,14]. The ratio of SnO to SnO_2 in the heterostructure could be tuned by adjusting the oxidation conditions [8,13]. Li et al. reported that p-n heterojunction sensors with SnO-SnO_2 nanocomposites exhibited a response of 8 at 50 ℃ toward 50 ppm NO_2 detection [14]. Zhao et al. developed a SnO/SnO_2 quantum dot-based sensor with a response of 15.9 at 200 ℃ with 50 ppm NO_2 gas [15].

Despite the superior characteristics of the SnO/SnO_2 heterostructure, the development of heterojunction chemiresistive NO_2 gas sensors remains challenging owing to their relatively low responses. Increasing defect sites for the generation of oxygen vacancies in the SnO/SnO_2 heterostructure is one of the methods to overcome the limitation of the NO_2 gas sensors. Oxygen vacancies have a significant influence on the electronic states and physical properties of the SnO/SnO_2 heterostructure, enhancing the binding energy and chemisorption effect with adsorbed oxygen molecules and increasing electron transport ability (from electrons in the conduction band to adsorbed oxygen molecules) [6,13,16].

Similarly, in this study, we developed a SnO/SnO_2 heterostructure NO_2 gas sensor with extrinsic oxygen vacancies, and compared its gas-sensing performance with that of a general SnO/SnO_2 gas sensor. SnO/SnO_2 particles were thermally treated in at H_2 atmosphere to induce a reducing reaction after a one-step hydrothermal synthesis processing to create an oxygen-vacancy rich condition in the SnO/SnO_2 heterostructure. In particular, oxygen defect sites were predominantly created in the SnO crystal phase with (00*h*) lattice planes in the heterostructure. The defect-rich SnO/SnO_2 heterostructure sensor showed superior sensing properties in the detection of NO_2: a high response (100.86) with a fast response time (t_{rep} = 5.83 s) and excellent selectivity (approximately 23 times higher than those of other target gases) to 50 ppm NO_2 at 150 ℃. Raman, electron paramagnetic resonance (EPR), X-ray photoelectron spectroscopy (XPS), and time-of-flight secondary ion mass spectrometry (ToF-SIMS) analyses indicated the presence of oxygen vacancies in the defect-rich SnO/SnO_2 crystal, which acted as effective electron donors for the adsorbed oxygen molecules and the NO_2 target gas. We believe that the direct formation of oxygen vacancies in the SnO/SnO_2 heterostructure allows for the creation of an efficient NO_2 gas sensor.

2. Experimental section

2.1. Chemical reagents

Tin(II) chloride dihydrate ($SnCl_2$·2 H_2O, ACS reagent, 98%), *N,N*-dimethylformamide (DMF, anhydrous, 99.8%), and sodium hydroxide (NaOH, reagent grade, ≥ 98%) were purchased from Sigma-Aldrich. All chemicals were obtained and used without further purification. Distilled water (di-water) and ethanol (95% extra pure) were obtained from Thermo Fisher Scientific Inc.

2.2. Synthesis of SnO/SnO_2 and defect-SnO/SnO_2 heterostructures

To synthesize a SnO/SnO_2 heterostructure, 1 g of $SnCl_2$·2 H_2O was added into a 25 mL di-water. The precursor solution was mixed at room temperature for 15 min to dissolve the salt completely. After 15 min, 12 mL of dimethylformamide (DMF) and 500 mg of NaOH were added to the precursor solution and blended for 30 min. The homogeneous solution was obtained, transferred into a Teflon-lined stainless-steel autoclave (100 mL), and placed in a preheated oven at 180 °C for 18 h. After cooling to room temperature, SnO/SnO_2 heterostructure particles were obtained by washing multiple times with di-water and ethanol in a centrifuge process (3900 rpm, 10 min) and drying in the oven at 70 °C overnight.

For a defect-SnO/SnO_2 heterostructure, the synthesized SnO/SnO_2 heterostructure particles were heat-treated in a furnace at 350 °C under an H_2 environment (5 cmol/mol, N_2 balance gas) for 1 h (heating rate is 5 °C/min). After the heat treatment, the furnace was cooled to room temperature.

2.3. General characterization

The particle shape information of the synthesized SnO/SnO_2 heterostructures, including the defect particles was obtained using field-emission scanning electron microscopy (FE-SEM, JEOL-7800F). The internal lattice phases of the particles were characterized by high-resolution transmission electron microscopy (HR-TEM) at an acceleration voltage of 200 kV (JEM-ARM200F NEO ARM, JEOL Ltd.,). X-ray diffraction (XRD; Bruker D8 Advance X-ray diffractometer; Cu Kα radiation, λ = 1.541 Å) patterns provide crystal lattice profiles for the (defect)-SnO/SnO_2 particles. The phase identification of SnO and SnO_2 in the particles was performed using a Raman spectrometer (Horiba Jobin-Yvon LabRAM) with an Ar-ion laser beam (excitation source: a wavelength of 532 nm). Electron paramagnetic resonance (EPR) spectra were recorded at a low temperature (4 K) using at Bruker EMXplus spectrometer (microwave frequency of 9.65 GHz, modulation frequency of 100 kHz, and modulation amplitude of 10 G). For the NO_2 non-reacted samples, X-ray photoelectron spectroscopy (XPS) measurement was performed with a K-alpha system using a monochromatic Al Kα irradiation of 1486.6 eV (Thermo Fisher Scientific). The XPS spectra were calibrated by setting a C 1 s peak at 284.9 eV. For the NO_2 exposed samples, (near) ambient-pressure XPS measurement was conducted using an XPS measurement instrument equipped with a PHOIBOS 150 electron analyzer and an exchangeable gas-flow cell (~700 mL volume). A micro-focused X-ray source (ca. 300 μm of beam size, Al Kα) was utilized and was delivered through a SiN window (16 mm X 10 mm). The NO_2 gas has flowed for 300 s in the cell that had a sample and then the XPS measurement was carried out. Time-of-flight secondary ion mass spectrometry (ToF-SIMS) depth profiles and 3D tomography were analyzed using a hybrid instrument of ToF-SIMS 5 spectrometer and ION-TOF (ion sources: Cs^+ ion gun with an acceleration voltage of 1 kV and Bi_3^+ ions with an acceleration voltage of 30 kV).

2.4. Fabrication and measurement of (defect)-SnO/SnO_2 heterostructure sensor devices

Interdigitated electrodes (IDEs) comprising Cr and Au with thicknesses of 5 nm and 100 nm, respectively, were patterned on a Si/SiO_2 substrate (10 × 5 mm^2) using the photo-lithographic method [17] and thermal deposition. The width of each electrode and the gap between them are 20 μm and 5 μm, respectively. The synthesized (defect)-SnO/SnO_2 heterostructures as a powder were dispersed in ethanol with a 1 mg mL^{-1} concentration for 30 min by ultrasonication. The powder solution (a black homogeneous dispersion) was sprayed out on the IDEs with an air-brush process for 5 min via heating the substrate at 100 °C.

The gas sensing properties of the (defect)-SnO/SnO_2 heterostructured sensor devices were tested using a customized sensing measurement system with four-channel gas lines (each line has 6∅ diameter). The system had a tube furnace (quartz tube, 25∅ diameter) in which a sensor device was mounted and connected to mass flow controllers (MFCs). The operating temperature of 100–400 °C with an interval of 50 °C was adjusted by a temperature controller (an error range of ±0.5 °C) connected to the tube furnace. The target gas, including other test gases (all gases were dry with nitrogen balance gas) were diluted to the standard gas (80% nitrogen and 20% oxygen) with dry air and used with a concentration of 50 ppm. To study the gas sensing response toward various concentrations of the target gas, we balanced specific concentrations (2.5–50 ppm) of the target gas with the standard gas. The total flow rate of the gas injected into the tube furnace was set to 1000 sccm. The electrical sensing resistance was monitored using a current source (Keithley 6220) and a nanovoltmeter (Keithley 2182) at a constant current of 10 nA with a time interval of 1 s in a LabView

environment.

3. Results and discussion

A one-pot hydrothermal process was used to obtain the SnO/SnO_2 heterostructure, including defect formation, as described in the Experimental Section (Fig. 1a). Sn^{2+} ions from $SnCl_2{\cdot}2\,H_2O$ were initially created in the di-water, and NaOH assisted in the nucleation of SnO/SnO_2 crystals. Heat treatment in a reducing atmosphere enables the formation of vacancy-rich SnO/SnO_2 structures [18]. For simplicity, hereinafter, the vacancy-rich SnO/SnO_2 crystals will be referred as 'defect-SnO/SnO_2 crystals'.

The structural morphology of the synthesized SnO/SnO_2 heterostructures was evaluated using scanning electron microscopy (SEM) (Fig. 1b-c). Both (defect)-SnO/SnO_2 crystals exhibited quadrangular structures tens of microns in size. It suggests that the gas molecules have effective chemical interactions with the micron-sized surfaces of the SnO/SnO_2 particles. Raman spectra of Fig. S1a prove the SnO/SnO_2 heterostructure. Two strong Raman peaks were observed at 112 and 201 cm^{-1}, corresponding to the E_g and $A_{1\,g}$ vibration modes of SnO, respectively [19,20]. Furthermore, new Raman modes slightly appeared at 140 and 170 cm^{-1} that can be ascribed to SnO_2 [19]. A SnO/SnO_2 heterostructure was designed for the SnO particles including SnO_2 phases. The internal morphology (TEM, Fig. S1b-c) shows the crystal lattice phases arising from SnO or SnO_2, and selected area electron diffraction (SAED) patterns provide detailed lattice information (Fig. 1d-e). Compared with the SnO/SnO_2 heterostructure, the defect-SnO/SnO_2 crystal exhibited partially different lattice phases according to the diffraction spots that can be indexed as the (111), (220), (311), and, (321) planes. This result indicates that the vacancy-rich condition in the defect-SnO/SnO_2 particle allows lattice deformation, which creates different crystal phases in the structure. It was confirmed by XRD analysis, as shown in Fig. 1f. The diffraction profiles in both (defect)-SnO/SnO_2 heterostructure particles showed predominantly polycrystalline SnO crystal phases (JCPDS No. 01–085–0712, blue triangle) [21] and a (110) lattice plane of tetragonal rutile-type SnO_2 structure at 26.78° as a two-theta peak (JCPDS No. 01–071–5324, green square, Fig. S2a) [22]. Interestingly, however, the peak intensities of the main Bragg reflections such as (001), (101), (110), (002), and (112) planes from the SnO crystal decreased in the defect-SnO/SnO_2 heterostructure (Fig. S2b-c). In particular, the diffraction intensities of the lattice plane of (001) and (002), which grew vertically along the Z-axis, were considerably reduced (Fig. S2c and inset). The XRD data indicate that the defect structure of the SnO/SnO_2 heterostructure resulted in low crystallinity in the SnO crystal phases including the (00 *h*) plane [23]. Therefore, defects mainly form in the (00 *h*) lattice planes of the SnO crystal. The formation of defects in the metal oxide structure induced the formation of oxygen vacancies in the crystal frame. It was confirmed in

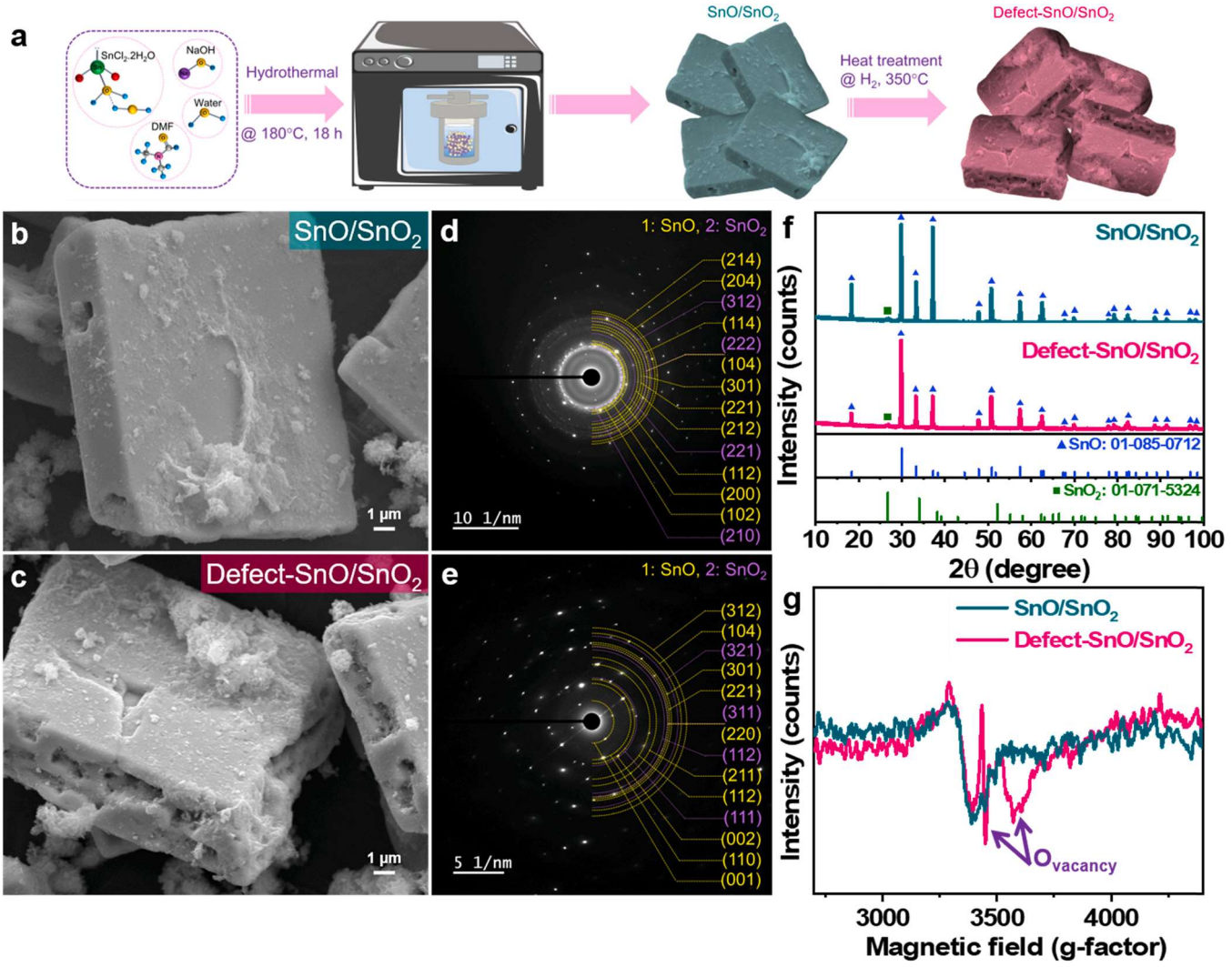

Fig. 1. Synthesis of SnO/SnO_2 heterostructure and defect-SnO/SnO_2 particles: (a) Schematic illustration of the synthetic route, (b and c) SEM images, (d and e) SAED patterns (Fig. 1b and d, upper panel: SnO/SnO_2 particles and Fig. 1c and e, lower panel: defect-SnO/SnO_2 particles) (f) XRD patterns, and (g) EPR spectra.

the EPR signals (Fig. 1g), which indicated the change in the valence states of O in the (defect)-SnO/SnO_2 heterostructures. From $E = g\beta_e B_0$, where h is Planck's constant (6.626×10^{-27} erg-s/cycle), ν is the frequency, β_e is Bohr magneton (9.274×10^{-21} erg/Gauss), and B_0 resonance magnetic field [24,25], the defect-SnO/SnO_2 crystal exhibited two distinct resonances at $g = 1.94$ and 2.00. It demonstrates the presence of electron donor oxygen vacancies in the crystal structure [24,26]. The defect formation in the SnO/SnO_2 crystal caused a reduction in the direct band gap (Fig. S3). The SnO/SnO_2 heterostructure showed a band gap of 3.27 eV (a reasonable value within the range of 2.5 – 3.6 eV [5, 7]), whereas the defect-SnO/SnO_2 showed 3.07 eV [27]. The reduced band gap lowers the potential barrier, making electron transfer more efficient from the conduction band to the valence band [28]. We expect that the defect-SnO/SnO_2 crystal may enhance sensing performance due to the defects, allowing more efficient chemical interactions with target gas and effective electron transfer by the reduced band gap.

From the SnO/SnO_2 material properties, we understand that 1) the SnO/SnO_2 and defect-SnO/SnO_2 heterostructures have a micron-sized particle structure, 2) the heterostructures are created to a mainly SnO crystal including SnO_2 phases, and 3) defects that arise from oxygen vacancies are predominantly generated in the (00 h) lattice phase of the SnO crystal.

Based on the SnO/SnO_2 and defect-SnO/SnO_2 heterostructure crystals, we tested the gas-sensing performance for the detection of NO_2 gas. The defect-SnO/SnO_2-based gas sensor had superior sensing properties, particularly response and selectivity, compared with the SnO/SnO_2-based sensor device. Both (defect)-SnO/SnO_2 crystals were deposited on IDEs, and chemiresistive sensor devices were created. We first investigated temperature-dependent sensing properties for the 50 ppm NO_2 and obtained resistance dynamics (temperature range: 100–400 °C). As shown in Fig. 2a, both sensors exhibited a resistance change time of 300 s and a variation in the initial resistance level in air (R_a) as a function of the operating temperature. R_a decreased as the temperature increased, because of the increase in the number of carriers with sufficient energy to overcome the potential barrier [29]. The initial resistance of 593 MΩ (max. at 100 °C) decreased to 221 KΩ (min. at 400 °C) for the SnO/SnO_2 heterostructure-based sensor, whereas that of the defect-SnO/SnO_2-based device showed a reduction from 37.8 MΩ to 96 KΩ. The low resistance levels in overall in the defect-SnO/SnO_2 heterostructure-based sensor indicate the reduction in the band gap because the generation of extrinsic oxygen defects in the heterostructure reduces the potential barrier for the movement of electrical carriers [29, 30]. After 300 s, the resistance levels of both sensors increased with temperature dependency when NO_2 gas was exposed. In the response results converted from the resistance values, more obvious temperature-dependent sensing performances were observed (Fig. S4). The response (S_{rep}) was calculated using the following equation: $S_{rep} = [(R_a - R_g)/R_a]$ where R_a and R_g are the resistances of the sensors in air and target gas, respectively [31]. The defect-SnO/SnO_2 crystal-based device showed a high response at a lower operating temperature; the SnO/SnO_2 heterostructure sensor exhibited a maximum response of 25.12 at 200 °C, whereas the defect-SnO/SnO_2 heterostructure sensor

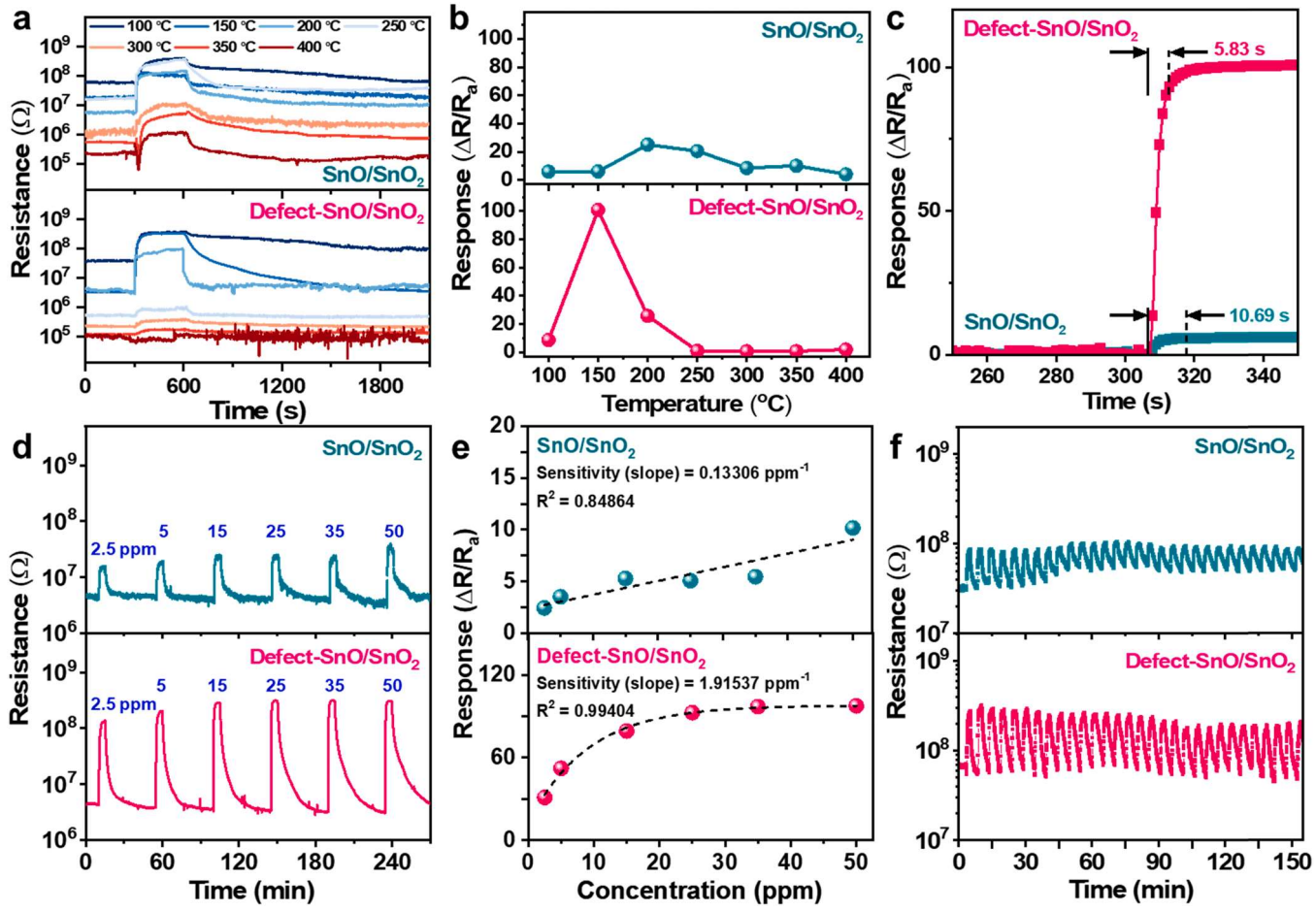

Fig. 2. Gas sensing performances of the sensors based on SnO/SnO_2 heterostructure or defect-SnO/SnO_2 crystals: (a) Temperature-dependent resistance dynamics and (b) corresponding response trends (NO_2, 50 ppm), (c) transient response results in the selective response curves at 150 °C, (d) the real-time resistance variations to NO_2 target gas with an increase in concentration at 150 °C, (e) NO_2 concentration (2.5–50 ppm) -sensing response relations, and (f) repeated sensing transients with 30-cycle resistance.

recorded that of value to 100.86 at 150 ℃. We understand that the oxygen defects in the SnO/SnO_2 heterostructure crystal not only encourage the adsorption of NO_2 molecules at a lower temperature but also enhance the electron transition from the SnO/SnO_2 crystal to the adsorbate [16]. Furthermore, with responses at other operating temperatures, we observed a mild response trend in the SnO/SnO_2-based device and a pointed response trend at 150 ℃ in the defect-SnO/SnO_2-based sensor (Fig. 2b). Fig. 2c exhibits transient response times that were evaluated [31,32] from the selected response curves at 150 ℃ for 50 ppm NO_2(highlighted in the time range of 250–350 s). The response times of the SnO/SnO_2 crystal and defect-SnO/SnO_2 heterostructure sensors were revealed to be 10.69 s and 5.83 s, respectively. The transient response time of approximately 5 s is a quite fast response rate for the detection of NO_2 molecules, making it an efficient NO_2 gas sensor.

Fig. 2d depicts the resistance dynamics depending on NO_2 concentrations at 150 ℃. Depending on the NO_2 concentration from 2.5 to 50 ppm, the resistance levels gradually increased in both (defect)-SnO/SnO_2 heterostructure sensor devices. They showed excellent response and recovery characteristics at each concentration under gas-in and -out conditions. The relationship between NO_2 concentration and the response is summarized in Fig. 2e. For the SnO/SnO_2 sensor, the responses depending on the concentrations showed a linear relation with a coefficient of $R^2 = 0.84864$. In contrast, the response of detect-SnO/SnO_2 sensor linearly increased up to 25 ppm, but the response was almost saturated at a concentration higher than 25 ppm. It reveals that the chemical interaction between NO_2 and defect-SnO/SnO_2 heterostructure might be maximized at the 25 ppm concentration. The detect-SnO/SnO_2 sensor system can be accurately described by the Langmuir isotherm model [33], which was well-fitted with a coefficient of $R^2 = 0.99404$. Fig. 2f shows the response and recovery sensing curves with 30 repeatable cycles for both sensors, which were exposed to 50 ppm NO_2 gas at 150 ℃. For the SnO/SnO_2-based sensor, the variation in resistance was 32%, which is lower than that in the initial state. The defect-SnO/SnO_2 sensor represented a stable sensing reaction.

High selectivity, particularly for the exclusive detection of a target gas, is one of the crucial factors in determining an efficient gas sensor. In Fig. 3a-b, both (defect)-SnO/SnO_2 chemiresistive sensors showed selectivity results for NO_2 gas that were compared with other test gases (50 ppm concentration). They exhibited considerably low responses (below 4) for the detection of NO, H_2, HCHO, CH_4, acetone, and styrene. However, the defect-SnO/SnO_2 crystal sensor showed a response almost 23 times higher and the SnO/SnO_2 crystal sensor showed approximately 5 times higher chemical reaction in the detection of NO_2 gas molecules. The highly exclusive NO_2 detection in the defect-SnO/SnO_2 sensor device is highlighted in comparison with previously reported SnO_x-based NO_2 gas sensors as shown in Fig. 3c. Other reported NO_2 gas sensors showed a response range of 0 – 20 for NO_2 concentrations of up to 100 ppm [34–40]. In the $SnO\text{-}SnO_2$ hybrid-based sensor, the response level was 16.7 toward even 100 ppm NO_2 [38]. However, the defect-SnO/SnO_2 heterostructure device exhibited a six times higher value at a low NO_2 concentration of 50 ppm. In brief, we argue that the defect-SnO/SnO_2 chemiresistive sensor device was designed to be an effective NO_2 gas sensor.

One of the reasons for the high sensing performances of the defect-SnO/SnO_2 sensor devices, is the chemical interaction between the sensing material of SnO/SnO_2 and the NO_2 target gas. We investigated the surface chemical composition of (defect)-SnO/SnO_2 heterostructures before and after NO_2 gas flow using XPS (Fig. 4). In the Sn-related states before NO_2 interaction (Fig. 4a), the Sn 3d spectrum of the SnO/SnO_2 crystal shows spin-orbit double peaks for the Sn $3d_{5/2}$ (low energy) and Sn $3d_{3/2}$ (high energy) state, respectively, which can be deconvoluted into two peaks centered at approximately 486.3 eV (Sn^{4+} $3d_{5/2}$) and 486.4 eV (Sn^{2+} $3d_{5/2}$) for the first peak and approximately 493.4 eV (Sn^{4+} $3d_{3/2}$) and 493.2 eV (Sn^{2+} $3d_{3/2}$) for the higher energy peak [41]. For the two main peaks arising from the discrepancy in the binding energies of the Sn–O bonds [42], the predominant moiety was Sn^{2+} due to the larger oxidation states of SnO phase superiority in the heterostructure crystal. These phenomena were observed in the defect-SnO/SnO_2 crystal; however, the spectrum was shifted to a lower binding energy (0.31 eV) that is attributed to the defect formation in the SnO/SnO_2 heterostructure [43–45], corresponding to electron transformation [46]. The larger chemical coupling with oxygen molecules in

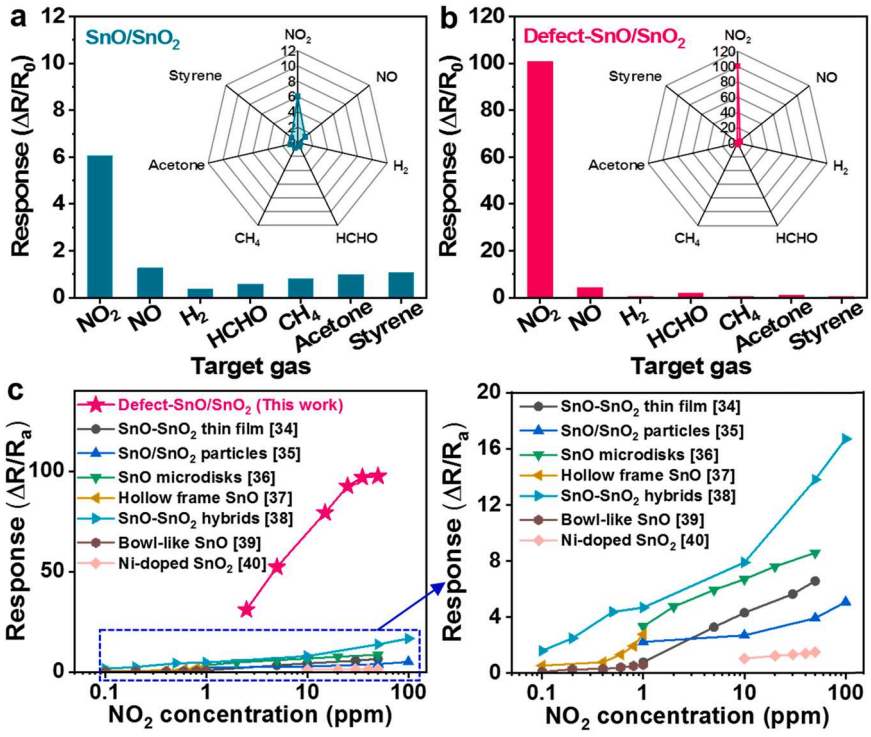

Fig. 3. Selectivity histogram from gas-sensing responses of (a) SnO/SnO_2 crystal- and (b) defect-SnO/SnO_2 crystal-based gas sensor toward various test gases with a concentration of 50 ppm. (c) Our sensor device highlighted in comparison with previous works by other research groups [reference #: –34,40] (target gas for NO_2).

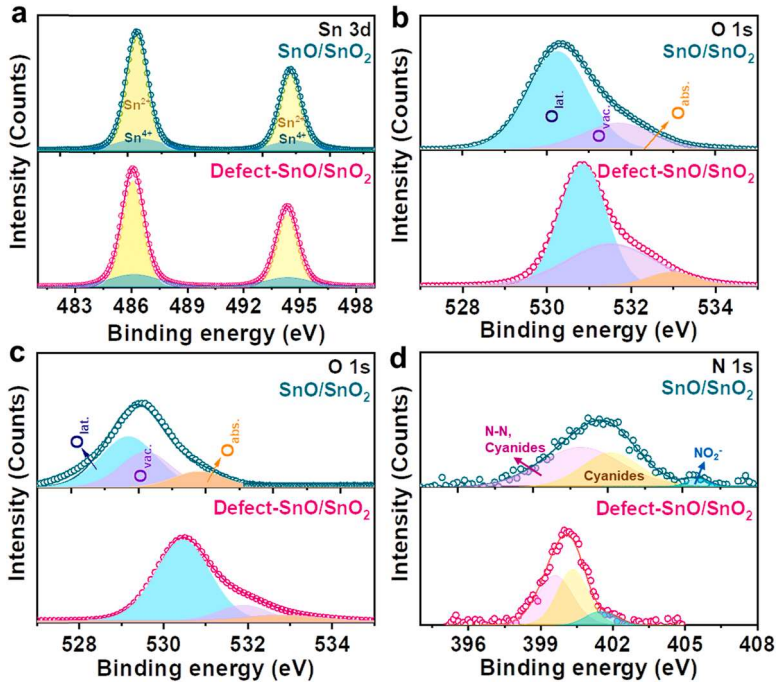

Fig. 4. XPS surface spectra of (defect)-SnO/SnO_2 heterostructure crystals before (first row) and after (second row) NO_2 interaction at 150 °C: (a) Sn 3d, (b and c) O 1 s, and (d) N 1 s.

the defect-SnO/SnO_2 crystal was confirmed by the O 1 s state in Fig. 4b (before NO_2 flow). Compared with the SnO/SnO_2 heterostructure, a positive shift of 0.49 eV in the defect-SnO/SnO_2 heterostructure was revealed according to the larger Sn–O ion interactions. Both O 1 s spectra consist of three components in different oxygen chemical states: $O_{lat.}$, $O_{vac.}$, and $O_{abs.}$ The $O_{lat.}$ demonstrates oxygen ions of the Sn–O bonds in the SnO/SnO_2 crystal (low energy curve - blue). The $O_{vac.}$ refers to the adsorbed oxygen ions adsorbed in the oxygen vacancy regions of the crystal (intermediate energy curve - purple). The $O_{abs.}$ shows the chemisorbed oxygen ion species e.g., O_2 or OH groups on the (defect)-SnO/SnO_2 crystal surface (high energy curve - orange) [47,48]. The higher fraction of $O_{abs.}$ in the defect-SnO/SnO_2 crystal supports the existence of more oxygen defects in the structure [49]. The higher $O_{vac.}$ level with approximately 48% of the area fraction in the defect-SnO/SnO_2 crystal (36% of the area fraction in the SnO/SnO_2 crystal) proves the higher sensing response because the oxygen vacancies donate electrons to the oxygen molecules, and interact with the target gas molecules [50].

Interestingly, after the NO_2 gas flow, we understand that 1) adsorbed oxygen molecules on the surfaces of the (defect)-SnO/SnO_2 crystals have chemical interactions with NO_2 molecules and 2) effective interactions occur in the defect-SnO/SnO_2 crystal. In the O 1 s states (Fig. 4c), the intensity of the binding energy related to oxygen bonds/ions on the surface and/or internal interaction in the SnO/SnO_2 heterostructure was considerably reduced compared with the non-NO_2 interactions of Fig. 4b. Furthermore, the shift in the binding energy to lower position indicates interactions between Sn and O [51]. These results indicate that the NO_2 molecules have surface interactions with the (defect)-SnO/SnO_2 heterostructure. The $O_{vac.}$ fraction values prove the effective NO_2 adsorption of the defect-SnO/SnO_2 crystal in the gas-sensing reaction; approximately 36.45% of the area fraction for the SnO/SnO_2 crystal and approximately 22.03% of the area fraction for the defect-SnO/SnO_2 crystal. The smaller $O_{vac.}$ fraction indicates that NO_2 molecules effectively govern the oxygen defect sites in the crystal structure. Fig. 4d provides the N 1 s states after the NO_2 reaction. In both (defect)-SnO/SnO_2 heterostructures, the spectra contain three deconvoluted peaks at approximately 398.6 eV, 399.4 eV, and 403.9 eV corresponding to the N–N bond, cyanide ($C \equiv N^-$), and NO_2^- [47,48]. The NO_2^- area fraction (blue curve) indicates that the defect-SnO/SnO_2 crystal (17.36%, the SnO/SnO_2 is for 5.72%) has more effective chemical interactions with NO_2 molecules, in particular, surface oxygen molecules on the crystal [52].

From the XPS results, we can conclude that higher NO_2 gas-sensing reaction occurred in the defect-SnO/SnO_2 heterostructure. To directly observe the NO_2 reaction, we conducted a ToF-SIMS analysis of the (defect)-SnO/SnO_2 crystal after NO_2 gas flow (measurements were performed using the heterostructured particles created into the sensor devices). $SnNO_2^-$, $SnNO^-$, and NO_2^- ion species were monitored, and they were evaluated a depth profiling (Fig. 5a-b). The dynamic $SnNO^-$ and NO_2^- variations as a function of the film depth were observed in the defect-SnO/SnO_2 heterostructure, whereas flat profilings for the $SnNO^-$ and NO_2^- ions were revealed in the SnO/SnO_2 heterostructure. This indicates that NO_2 molecules reacted effectively on the SnO/SnO_2 crystal with defect-rich phases for chemical interaction, which remained in the middle position of the crystal [53]. This result is visualized in the three-dimensional (3D) tomography images of Fig. 5c. The dominant $SnNO^-$ and NO_2^- fragments were positioned near the surface of the defect-SnO/SnO_2 crystal because NO_2 molecules interacted with the surface adsorbed oxygen species that communicated with the SnO/SnO_2 compounds in the defect containing crystal structure.

4. Conclusions

In this work, we designed SnO/SnO_2 heterostructured crystals with and without defect-rich phases. The (defect)-SnO/SnO_2 particles were formed SnO crystals, including the SnO_2 lattice phase. Defect sites were mainly generated in the (00 *h*) phases of the crystal. The defect-SnO/SnO_2 heterostructure-based gas sensor showed superior sensing properties in the detection of the NO_2 target gas (50 ppm at 150 °C); a high response of 100.86, fast response time of 5.83 s, and excellent selectivity (approximately 23 times higher than those of other target gases). These sensing performance values were remarkable compared to those of the SnO/SnO_2-based gas sensor (50 ppm at 200 °C, response = 25.12, transient response time = 10.69 s, and 6 times higher selectivity than

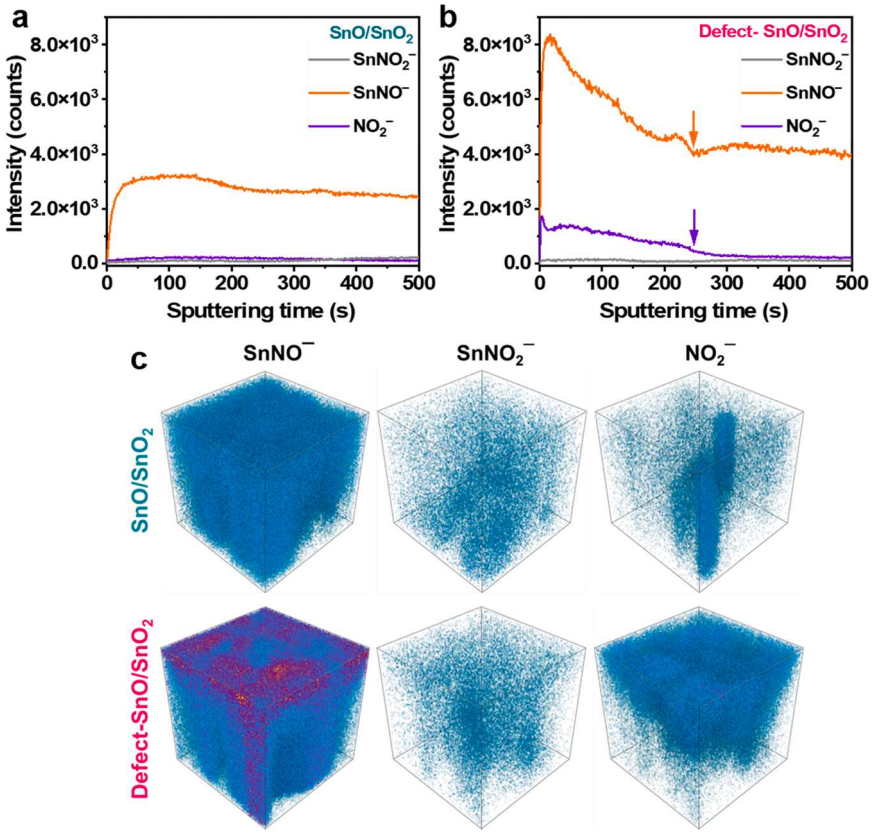

Fig. 5. Probing chemical interactions of NO_2 molecules with (defect)-SnO/SnO_2 heterostructures: TOF-SIMS analysis including 1D-profiling curves (a and b) and (c) 3D-tomography results for $SnNO^-$, $SnNO_2^-$, and NO_2^- distributions.

other test gases). The extrinsic formation of oxygen vacancies in the SnO/SnO_2 heterostructure reduces the energy bandgap, which can adjust the potential barrier, allowing an easier electron transfer from the conduction band to the adsorbed oxygen species. XPS and ToF-SIMS analyses proved effective NO_2 interactions in the NO_2 gas flow environment. Therefore, we suggest a direct design of the extrinsic oxygen defects in the SnO/SnO_2 heterostructure and their significant effects on sensing performance. We believe that this study will have a ripple effect on the development of SnOx-based NO_2 gas sensors.

CRediT authorship contribution statement

Jihee Kim: Methodology, Validation, Investigation, Data curation, **Masoud Nazarian-Samani:** Conceptualization, Methodology, Validation, Investigation, Data curation, Writing - original draft **Jihyun Lee:** Data curation, Formal analysis **Sang-kil Lee:** Data curation, Formal analysis **Ji Hee Pi:** Methodology **Kyu Hyong Lee:** Investigation, Resources **Yu Jin Kim:** Writing - review & editing, Supervision **Sanghyeon Lee:** Writing - review & editing, Data curation **Wooyoung Lee:** Supervision, Resource, Project administration, Funding acquisition.

Declaration of Competing Interest

The authors declare that they have no known competing financial interests or personal relationships that could have appeared to influence the work reported in this paper.

Data availability

Data will be made available on request.

Acknowledgments

This work was supported by the Technology Innovation Program (‘20013621′, Center for Super Critical Material Industrial Technology) funded By the Ministry of Trade, Industry & Energy (MOTIE, Korea). This research was supported by the National Research Foundation of Korea (NRF) grant funded by the Korea government (MIST) (No. NRF-2022M3H4A3053304, National Core Materials Research Center (Platform type)). This research was also supported by the Basic Science Research Program and the Korea Initiative for fostering University of Research and Innovation (KIURI) Program through the National Research Foundation of Korea (NRF) funded by the Ministry of Education (NRF-2019R1A6A1A11055660) and the Korean government (MSIT) (NRF-2020M3H1A1077207).

Appendix A. Supporting information

Supplementary data associated with this article can be found in the online version at doi:10.1016/j.snb.2023.134751.

References

[1] S.A. Vanalakar, V.L. Patil, N.S. Harale, S.A. Vhanalakar, M.G. Gang, J.Y. Kim, P. S. Patil, J.H. Kim, Contolled growth of ZnO nanorod arrays via wet chemical route for NO_2 gas sensor applications, Sens. Actuators B: Chem. 221 (2015) 1195.
[2] Q. Li, W. Zeng, Y. Li, Metal oxide gas sensors for detecting NO_2 in industrial exhaust gas: recent developments, Sens. Actuators B: Chem. 359 (2022), 131579.
[3] Z. Peng, L.-Q. Tao, S. Zou, C. Zhu, G. Wang, H. Sun, T.-L. Ren, A multi-functional NO_2 gas monitor and self-alarm based on laser-induced graphene, Chem. Eng. J. 428 (2022), 131079.
[4] K. Wetchakun, T. Samerjai, N. Tamaekong, C. Liewgurab, C. Siriwong, V. Kruefu, A. Wisitsoraat, A. Tuantranont, S. Panichphant, Semiconducting metal oxides as sensors for environmentally hazardous gases, Sens. Actuators B: Chem. 160 (2011) 580.

[5] Y. Ogo, H. Hiramatsu, K. Nomura, H. Yanagi, T. Kamiya, M. Hirano, H. Hosono, P-channel thin film transistor using p-type oxide semiconductor, SnO, Appl. Phys. Lett. 93 (2008), 032113.

[6] A. Shanmugasundaram, P. Basak, L. Satyanarayana, S.V. Manorama, Hierarchical SnO/SnO_2 nanocomposites: formation of in situ p–n junctions and enhanced H_2 sensing, Sens. Actuators B: Chem. 185 (2013) 265.

[7] K.-M. Li, Y.-J. Li, M.-Y. Lu, C.-I. Kuo, L.-J. Chen, Direct conversion of single-layer SnO nanoplates to multi-layer SnO_2 nanoplates with enhanced ethanol sensing properties, Adv. Funct. Mater. 19 (2009) 2453.

[8] L. Meng, W. Bu, Y. Li, Q. Qin, Z. Zhou, C. Hu, X. Chuai, C. Wang, P. Sun, G. Lu, Highly selective triethylamine sensing based on SnO/SnO_2 nanocomposite synthesized by one-step solvothermal process and sintering, Sens. Actuators B: Chem. 342 (2021), 130018.

[9] N. Goel, K. Kunal, A. Kushwaha, M. Kumar, Metal oxide semiconductors for gas sensing, Eng. Rep. 5 (2023), e12604.

[10] A. Khort, Y. Haiduk, I. Taratyn, D. Moskovskikh, K. Podbolotov, A. Usenka, N. Lapchuk, V. Pankov, High-performance selective NO_2 gas sensor based on In_2O_3-graphene-Cu nanocomposites, Sci. Rep. 13 (2023) 7834.

[11] K. Suganthi, E. Vinoth, L. Sudha, P. Bharathi, M. Navaneethan, Manganese (Mn^{2+}) doped hexagonal prismatic zinc oxide (ZnO) nanostructures for chemiresistive NO_2 sensor, Sens. Actuators B: Chem. 380 (2023), 133293.

[12] T.H. Eom, S.H. Cho, J.M. Suh, T. Kim, J.W. Yang, T.H. Lee, S.E. Jun, S.J. Kim, J. Lee, S.-H. Hong, H.W. Jang, Visible light driven ultrasensitive and selective NO_2 detection in tin oxide nanoparticles with sulfur doping assisted by L-cysteine, Small 18 (2022) 2106613.

[13] G. Yin, J. Sun, F. Zhang, W. Yu, F. Peng, Y. Sun, X. Chen, L. Xu, J. Lu, C. Luo, M. Ge, D. He, Enhanced gas selectivity induced by surface active oxygen in SnO/SnO_2 heterojunction structures at different temperatures, RSC Adv. 9 (2019) 1903.

[14] L. Li, C. Zhang, W. Chen, Fabrication of SnO_2-SnO nanocomposites with p-n heterojunctions for the low-temperature sensing of NO_2 gas, Nanoscale 7 (2015) 12133.

[15] J. Zhao, R. Tan, Y. Guo, Y. Lu, W. Xu, W. Song, SnO mesocrystals: additive-free synthesis, oxidation, and top-down fabrication of quantum dots, Cryst. Eng. Comm. 14 (2013) 4575.

[16] Y. Xu, L. Zheng, C. Yang, W. Zheng, X. Liu, J. Zhang, Oxygen vacancies enabled porous SnO_2 thin films for highly sensitive detection of triethylamine at room temperature, ACS Appl. Mater. Interfaces 12 (2020) 20704.

[17] J. Lee, Y. Choi, B.J. Park, J.W. Han, H.-S. Lee, J.H. Park, W. Lee, Precise control of surface oxygen vacancies in ZnO nanoparticles for extremely high acetone sensing response, J. Adv. Ceram. 11 (2022) 769.

[18] J.H. Yang, H.J. Lee, H.S. Lee, S.-C. Jeon, Y.-S. Han, Precise control of heat-treatment conditions to improve the catalytic performance of V_2O_5/TiO_2 for H_2S removal, J. Hazard. Mater. 416 (2021), 125974.

[19] X.W. Guo, X.P. Fang, Y. Sun, L.Y. Shen, Z.X. Wang, L.Q. Chen, Lithium storage in carbon-coated SnO2 by conversion reaction, J. Power Sources 226 (2013) 75.

[20] D.M. Jang, H. Jung, N.D. Hoa, D. kim, S.-K. Hong, H. Kim, Tin oxide-carbon nanotube composite for NOx sensing, J. Nano. Nanotechnol. 12 (2012) 1425.

[21] S.J. Han, S. Kim, J. Ahn, J.K. Jeong, H. Yang, H.J. Kim, Composition-dependent structural and electrical properties of p-type SnOx thin films prepared by reactive DC magnetron sputtering: effects of oxygen pressure and heat treatment, RSC Adv. 6 (2016) 71757.

[22] M.J. Mortelliti, C.-W. Huang, J.M. Atkin, J.L. Dempsey, Mixed tin-titanium oxides by atomic layer deposition on planar substrates: physical and electronic structure, Appl. Surf. Sci. 573 (2022), 151564.

[23] C.F. Holder, R.E. Schaak, Tutorial on powder X-ray diffraction for characterizing nanoscale materials, ACS Nano 13 (2019) 7359.

[24] M. Nazarian-Samani, M. Nazarian-Samani, S. Haghighat-Shishavan, K.-B. Kim, Fe^{3+}-derived boosted charge transfer in an $FeSi_4P_4$ anode for ultradurable Li-Ion Batteries, ACS Nano 16 (2022) 12606.

[25] M.M. Roessler, E. Salvadori, Principles and applications of EPR spectroscopy in the chemical sciences, Chem. Soc. Rev. 23 (2018) 2534.

[26] Y.-X. Zhen, B.-Y. Song, W.-X. Liu, J.-X. Ye, X.-F. Zhang, Z.-P. Deng, L.-H. Huo, S. Gao, Ultra-high response and low temperature NO_2 sensor based on mesoporous SnO_2 hierarchical microtubes synthesized by biotemplating process, Sens. Actuators B: Chem. 363 (2022), 131852.

[27] L. Liu, Y. Wang, Y. Liu, S. Wang, T. Li, S. Feng, S. Qin, T. Zhang, Heteronanostructural metal oxide-based gas microsensors, Microsyst. Nanoeng. 85 (2022) 85.

[28] S. Peng, Z. Wang, R. Liu, J. Bi, J. Wu, Controlled oxygen vacancies of $ZnFe_2O_4$ with superior gas sensing properties prepared via a facile one-step self-catalyzed treatment, Sens. Actuators B: Chem. 288 (2019) 649.

[29] B. Saruhan, R.L. Fomekong, S. Nahirniak, Review: influences of Semiconductor metal oxide properties on gas sensing characteristics, Front. Sens. 2 (2021), 657931.

[30] X. Wang, T. Wang, G. Si, Y. Li, S. Zhang, X. Deng, X. Xu, Oxygen vacancy defects engineering on Ce-doped α-Fe2O3 gas sensor for reducing gases, Sens. Actuators B: Chem. 302 (2020), 127165.

[31] K.G. Krishna, S. Parne, N. Pothukanuri, V. Kathirvelu, S. Gandi, D. Joshi, Nanostructured metal oxide semiconductor-based gas sensors: a comprehensive review, Sens. Actuators A: Phys. 341 (2022), 113578.

[32] D. Drix, M. Schmuker, Resolving fast gas transients with metal oxide sensors, ACS Sens. 6 (2021) 688.

[33] S. Gupta, A. Anand, Neeru, R. Kurmar, Study of adsorption kinetics of pristine and SnO_2 functionalized carbon nanotubes as environment gas sensors for NO_2 and NH_3 gases, Mater. Today.: Proc. 47 (2021) 1651.

[34] H.-S. Jeong, M.-J. Park, S.-H. Kwon, H.-J. Joo, S.-H. Song, H.-I. Kwon, Low temperature NO_2 sensing properties of RF-sputtered SnO-SnO_2 heterojunction thin-film with p-type semiconducting behavior, Ceram. Int. 44 (2018) 17283.

[35] P. Wang, W. Ge, X. Jia, J. Huang, X. Zhang, J. Lu, SnO/SnO_2 heterojunction: an alternative candidate for sensing NO_2 with fast response at room temperature, Front. Mater. Sci. 16 (2022), 220609.

[36] M.G. Masteghin, D.R.M. Godoi, M.O. Orlandi, Heating method effect on SnO micro-disks as NO_2 gas sensor, Front. Mater. 6 (2019) 171.

[37] Q. Ren, X. Zhang, Y. Wang, M. Xu, J. Wang, Q. Tian, K. Jia, X. Liu, Y. Sui, C. Liu, J. Yun, J. Yan, W. Zhao, Z. Zhang, Shape-controlled and stable hollow frame structures of SnO and their highly sensitive NO_2 gas sensing, Sens. Actuators B: Chem. 340 (2021), 129940.

[38] H. Yu, T. Yang, Z. Wang, Z. Li, Q. Zhao, M. Zhang, p-N heterostructural sensor with SnO-SnO_2 for fast NO_2 sensing response properties at room temperature, Sens. Actuators B: Chem. 258 (2018) 517.

[39] Q. Ren, X. Zhang, Y. Guo, M. Xu, H. Zhu, J. Yun, W. Zhao, Z. Zhang, Y. Wang, Shape-controlled SnO and their improved properties in the field of gas sensor, photocatalysis, and lithium-ion battery, Sens. Actuators B: Chem. 372 (2022), 132622.

[40] K.I.A. Wahid, C. Chaker, H. Chaker, Ni-doped SnO_2 thin films for NO_2 gas sensing application, Sens. Actuators B: Chem. 360 (2023), 114498.

[41] Y. Inomata, K. Albrecht, K. Yamamoto, Size-dependent oxidation state and CO oxidation activity of tin oxide clusters, ACS Catal. 8 (2018) 451.

[42] W.-d Zhou, D. Dastan, X.-t Yin, S. Nie, S. Wu, Q. Wang, J. Li, Optimization of gas sensing properties of n-SnO_2/p-xCuO sensors for homogeneous gases and the sensing mechanism, J. Mater. Sci: Mater. Electron 31 (2020) 18412.

[43] M. Shao, J. Liu, W. Ding, J. Wang, F. Dong, J. Zhang, Oxygen vacancy engineering of self-doped SnO_{2-x} nanocrystals for ultrasensitive NO_2 detection, J. Mater. Chem. C. 8 (2020) 487.

[44] Y. Xu, L. Zheng, C. Yang, W. Zheng, X. Liu, J. Zhang, Oxygen vacancies enabled porous SnO2 thin films for highly sensitive detection of triethylamine at room temperature, ACS Appl. Mater. Interfaces 12 (2020) 20704.

[45] S. Kucharski, P. Ferrer, F. Venturini, G. Held, A.S. Walton, C. Byrne, J. A. Covington, S.K. Ayyala, A.M. Beale, C. Blackman, Direct in situ spectroscopic evidence of the crucial role played by surface oxygen vacancies in the O_2- sensing mechanism of SnO_2, Chem. Sci. 13 (2022) 6089.

[46] G. Greczynski, L. Hultman, X-ray photoelectron spectroscopy: towards reliable binding energy referencing, Prog. Mater. Sci. 107 (2020), 100591.

[47] Y. Shi, T. Liu, Y. Zhao, J. Su, S. Zeb, Y. Nie, C. Qin, B. Wang, X. Jiang, Tunable oxygen vacancies of cobalt oxides for efficient gas sensing application, Sens. Actuators B: Chem. 350 (2022), 130860.

[48] R.G. Motsoeneng, I. Kortidis, S.S. Ray, D.E. Motaung, Designing SnO_2 nanostructure-based sensors with tailored selectivity toward propanol and ethanol vapors, ACS Omega 4 (2019) 13696.

[49] X. Wang, T. Wang, G. Si, Y. Li, S. Zhang, X. Deng, X. Xu, Oxygen vacancy defects engineering on Ce-doped α-Fe_2O_3 gas sensor for reducing gases, Sens. Actuators B: Chem. 302 (2020), 127165.

[50] M. Lee, M.Y. Kim, J. Kim, C.O. Park, H.E. Choa, S.Y. Lee, M.K. Park, H. Min, K. H. Lee, W. Lee, Conductometric sensor for gaseous sulfur-mustard simulant by gold nanoparticles anchored on ZnO nanosheets prepared via microwave irradiation, Sens. Actuators B: Chem. 386 (2023), 133726.

[51] K. Ganapathi S, M. Kaur, S. M, A. Pathak, S.C. Gadkari, A.K. Debnath, Highly sensitive NO_2 sensor based on ZnO nanostructured thin film prepared by SILAR technique, Sens. Actuators B: Chem. 335 (2021), 129678.

[52] J. Li, M. Yang, X. Cheng, X. Zhang, C. Guo, Y. Xu, S. Gao, Z. Major, H. Zhao, L. Huo, Fast detection of NO_2 by porous SnO_2 nanotoast sensor at low temperature, J. Hazard. Mater. 419 (2021), 126414.

[53] J. Ekar, P. Panjan, S. Drev, J. Kovac, ToF-SIMS depth profiling of metal, metal oxide, and alloy multilayers in atmospheres of H_2, C_2H_2, CO, and O_2, J. Am. Soc. Mass Spectrom. 33 (2022) 31–44.

Jihee Kim received a Bachelor's degree in Materials Science and Engineering from Pusan National University in 2021. She is a M.S candidate at the Department of Materials Science and Engineering in Yonsei University under the supervision of Prof. Wooyoung Lee. She is currently studying metal-oxide-semiconductor gas sensors.

Masoud Nazarian-Samani received his MSc in 2009 from the K.N. Toosi University of Technology, Iran, and his Ph.D. in 2017 from the University of Tehran, Iran, both in Materials Science and Engineering. He joined Yonsei University as a visiting Ph.D. student in December 2014. Additionally, he worked as a postdoctoral researcher at Yonsei University from October 2017 to April 2019 and as a research professor from May 2019 to March 2023. As of April 2023, he has moved to Sejong University, where he is working on the development of solid-state energy storage devices.

Jihyun Lee received a Bachelor's degree in Material Science and Engineering at Kookmin University in 2020. Since 2020, she is currently a Ph.D. candidate at the Department of Materials Science and Engineering at Yonsei University under the supervision of Prof. Wooyoung Lee. She is currently studying on nanostructured metal-oxide semiconductor gas sensors.

Sang-kil Lee received a Bachelor's degree in Material Science and Engineering at Yonsei University in 2023. Since 2023, he is currently studying on semiconductor gas sensors as a Master's student under the guidance of Prof. Wooyoung Lee at Yonsei University.

Ji Hee Pi received a master's degree in Materials Science and Engineering at Korea national University of Transportation in 2020. Since 2020, she is currently a Ph.D. candidate at the Department of materials Science and Engineering at Yonsei University under the supervision of Prof. Kyu Hyong Lee. She is studying on metal-oxide semiconductor sensors and the development of high-performance thermoelectric materials.

Kyu Hyong Lee is currently a professor in the Department of Materials Science and Engineering at Yonsei University in Seoul, Korea. He received his Ph.D. in ceramic engineering from Yonsei University in 2005. From 2005–2007, he worked as a postdoctoral research fellow at Nagoya University. Since 2007, he has been a research staff member and since 2010 project leader at the Samsung Advanced Institute of Technology. His research activity has focused on the development of high-performance thermoelectric materials and functional oxides.

Yu Jin Kim is a research professor in the Department of Materials Science and Engineering and a research institute of the Korea Initiative for Fostering University of Research and Innovation (KIURI). She received a Ph.D. degree from Pohang University of Science and Technology (POSTECH) in 2016 and started to work at Argonne National Laboratory as a Named-fellowship post-doc in the same year. From the end of 2019, she worked at Argonne as an assistant scientist in the Center for Nanoscale Materials and Argonne Photon Source. After 2 years, she moved to SLAC national accelerator laboratory and worked at Stanford Synchrotron Radiation Laboratory. She has expertise in X-ray science to investigate the internal information of semiconducting materials. Currently, she has mainly focused on the discovery of a sensing mechanism in sensor devices.

Sanghyeon Lee is a research staff in a research institute of the Korea Initiative for Fostering Univerisity of Research and Innovation (KIURI). He received a Ph.D. degree from Hanyang Univerisity in 2019. From 2019–2021, he worked as a postdoctoral research fellow at The Univerisity of Hong Kong. His research interests have focused on the fabrication of sensing devices using various deposition techniques.

Wooyoung Lee is the Underwood distinguished professor of the Department of Materials Science and Engineering at Yonsei University in Korea. He is also the Director of the Center for Super Critical Material Industrial Technology, National Core Materials Research Center and the institute of Korea Initiative for Fostering University of Research and Innovation. He is the President of The Korean Magnetics Society and a regular member of the National Academy of Engineering of Korea. In recent years, his research interests have centered on hydrogen sensors, various metal oxide semiconducting gas sensors, and breath analyzers. He is also studying rare-earth permanent magnets and thermoelectric materials and devices. He has received a number of awards in nano-related research areas including a Prime Minister Award (2023) in Nano Korea 2023, SeAH-Haiam Fellowship Award (2018) in The Korean Institute of Metals and Materials and a Service Merit Medal (2008) from the Government of Korea due to his contribution to the development of intellectual properties. He has authored and co-authored over 280 publications and has edited three special books on nanostructured materials and devices.